

# Crystallization of $\gamma$ -Fe<sub>2</sub>O<sub>3</sub> particles with the aid of barium oxide as a catalyst and the effects on magnetic properties

S. RAM, KUMAR A. NARAYAN\* ‡

Advanced Centre for Materials Science, and \*Department of Chemical Engineering,  
Indian Institute of Technology at Kanpur, Kanpur 208 016, India

$\gamma$ -Fe<sub>2</sub>O<sub>3</sub> particles with BaO additives (up to 20 mol%) have been crystallized by solid state reaction of the stoichiometric compositions containing 20 mol% B<sub>2</sub>O<sub>3</sub> as a sintering aid. This markedly effects the crystallization and magnetic properties of  $\gamma$ -Fe<sub>2</sub>O<sub>3</sub>. The microstructure of the samples shows growth of crystallites of considerably smaller sizes and with fairly sharp size distribution after the additions. Crystallites as small as  $\sim 5 \mu\text{m}$  size (normally 25  $\mu\text{m}$ ) were obtained using 15 to 20 mol% BaO additives in the reaction performed at 1230°C/20 h. This leads to a variation in coercivity over a wide range from 35 to 3500 Oe. Measurements of X-ray diffractometry, magnetization, microstructure and magnetic resonance have been carried out to characterize the magnetic applications of the material. The results are all consistent and elucidate promotion by thermal-treatment of the incorporation of Ba<sup>2+</sup> into the  $\gamma$ -Fe<sub>2</sub>O<sub>3</sub> particle cores.

## 1. Introduction

It has been observed that the coercivity and other intrinsic magnetic properties [1–4] of  $\gamma$ -Fe<sub>2</sub>O<sub>3</sub> can be significantly modified by the incorporation of suitable impurities. Yoshii *et al.* [1] synthesized  $\gamma$ -Fe<sub>2</sub>O<sub>3</sub> as thin films showing good uniformity of the material, as required for recording characteristics, by using titanium and copper cation additions. Experiments exploring the addition of BaO and B<sub>2</sub>O<sub>3</sub> using the solid reaction process are reported here. It should be noted that the BaO–Fe<sub>2</sub>O<sub>3</sub>–B<sub>2</sub>O<sub>3</sub> composition series, when studied by crystallization from the glass [5–7] gives rise to the crystallization of BaFe<sub>12</sub>O<sub>19</sub> ferrite particles. The BaO in the solid state reaction system incorporates (Ba<sup>2+</sup>  $\rightleftharpoons$  Fe<sup>3+</sup>) in  $\gamma$ -Fe<sub>2</sub>O<sub>3</sub> and suppresses the crystalline grain growth. B<sub>2</sub>O<sub>3</sub>, having a much lower melting temperature ( $\sim 460^\circ\text{C}$ ) than the temperatures used for the reaction ( $\geq 1100^\circ\text{C}$ ), behaves as a molten flux which facilitates the crystallization of barium-substituted  $\gamma$ -Fe<sub>2</sub>O<sub>3</sub> particles. The results are correlated with the development of coercivity and magnetic moments ( $M_s$ ) in the samples as a function of the thermal treatments for the reaction.

## 2. Experimental procedure

The barium-substituted  $\gamma$ -Fe<sub>2</sub>O<sub>3</sub> particles were prepared by high-temperature solid-state reaction of BaCO<sub>3</sub>, Fe<sub>2</sub>O<sub>3</sub> and B<sub>2</sub>O<sub>3</sub> mixed together (compositions are given in Table I) by ball milling in acetone. After drying, the samples were pressed to ribbons of 1  $\mu\text{m}$  thickness (by applying a pressure of  $\sim 8$  ton) and were sintered at temperatures ranging from 1000 to

1400°C to induce crystallization. The crystals were analysed by X-ray diffractometry and microstructure of the samples.

Magnetization measurements were performed on a PAR Vibrating Sample magnetometer (model 150) with an applied field up to 10 kOe (1 Oe =  $1/4\pi \times 10^3 \text{ A m}^{-1}$ ). The magnetic resonance spectra of the selected samples were measured with a Varian Associates spectrophotometer (model V-4502-12) in the X-band frequency region. The other experimental details are reported elsewhere [8].

## 3. Results and discussion

### 3.1. Crystallization of $\gamma$ -(Fe<sub>1-x</sub>Ba<sub>x</sub>)<sub>2</sub>O<sub>3</sub> particles (X-ray diffraction and microstructural aspects)

The  $\gamma$ -(Fe<sub>1-x</sub>Ba<sub>x</sub>)<sub>2</sub>O<sub>3</sub> particles readily crystallize out in the samples subjected to thermal treatments between 1000 and 1400°C, showing optimum crystallization yields for treatment at  $\sim 1230^\circ\text{C}$  for 20 h. The results obtained for the various samples after a given

TABLE I Compositions investigated with varying amounts of BaO (mol %) in the  $\gamma$ -(Fe<sub>1-x</sub>Ba<sub>x</sub>)<sub>2</sub>O<sub>3</sub> series

BaO	Fe <sub>2</sub> O <sub>3</sub>	B <sub>2</sub> O <sub>3</sub>	Expected value for x	Code
2	78	20	0.01	A
5	75	20	0.03	B
8	72	20	0.05	C
15	65	20	0.10	D
20	60	20	0.14	E

TABLE II The results of crystallization, particle size and magnetic parameters for the various samples\*

Sample	Crystallization yield (wt %)		Particle size ( $\mu\text{m}$ )	Magnetic parameters		
	Observed	Calculated		$M_s$ (e.m.u. $\text{g}^{-1}$ )	$H_c$ (Oe)	$M_r/M_s$
A	40	90.16	20	24	200	0.10
B	75	90.15	15	30	250	0.12
C	80	90.14	10	33	300	0.18
D	88	90.11	5	40	400	0.20
E	90	90.08	5	41	550	0.31

\* All samples were given thermal treatment at  $1230^\circ\text{C}/20\text{ h}$ . The particle size data indicate the average particle size. The particles of smaller sizes (up to  $0.5\ \mu\text{m}$ ) were produced for treatments at lower ( $\sim 1000^\circ\text{C}$ ) temperatures.

thermal treatment at  $1230^\circ\text{C}/20\text{ h}$  are summarized in Table II. Sample E, which contains 20 mol % BaO, gives a maximum crystallization of  $\sim 90\text{ wt}\%$ . This is very close to the theoretically calculated crystallization of  $\sim 90.08\text{ wt}\%$ , assuming 100% utilization of the BaO and  $\text{Fe}_2\text{O}_3$  contents in the crystallization of  $\gamma\text{-(Fe}_{1-x}\text{Ba}_x)_2\text{O}_3$ , with  $x \leq 0.1$ . Compositions containing BaO contents higher than 20 mol % were also tried but they did not show useful results. The maximum amount of BaO dissolved in the crystallites appears to be limited to  $x \sim 0.1$  (equivalent to 20 mol %).

TABLE III X-ray diffraction lines of  $\gamma\text{-Fe}_2\text{O}_3$

$d_{hkl}$ (nm)	$I/I_0$	$hkl$	$a_0 = 0.835\text{ nm}$
0.373	5	2 1 0	
0.295	34	2 2 0	
0.278	19	2 2 1	
0.264	—	3 1 0	
0.252	100	3 1 1	
0.241	1	2 2 2	
0.232	6	3 2 0	
0.223	0.5	3 2 1	
0.208	24	4 0 0	

Data are taken from JCPDS file 4.755.

The substitution of  $\text{Ba}^{2+}$  in  $\gamma\text{-Fe}_2\text{O}_3$  is evident by the modified X-ray diffraction patterns of  $\gamma\text{-Fe}_2\text{O}_3$  [9] shown for the various samples. An example of X-ray diffraction patterns for sample E (sintered at  $1230^\circ\text{C}/20\text{ h}$ ) is given in Fig. 1. The diffraction data for pure synthesized  $\gamma\text{-Fe}_2\text{O}_3$  are given in Table III for comparison. The  $\gamma\text{-(Fe}_{1-x}\text{Ba}_x)_2\text{O}_3$  particles essentially crystallize in a cubic crystal structure with lattice constant  $a_0 = 0.839\text{ nm}$ , which is significantly larger than  $a_0 = 0.835\text{ nm}$  for  $\gamma\text{-Fe}_2\text{O}_3$ , possibly due to the larger size of the  $\text{Ba}^{2+}$  cations.

Fig. 2 shows micrographs of typical samples containing 5, 8 and 20 mol % BaO. The average particle size of the sample with no BaO added is estimated (from the micrographs) to be  $25\ \mu\text{m}$ , and this was reduced to  $5\ \mu\text{m}$  after the addition of BaO. The barium oxide in these samples behaves as an internal catalyst, modifying the particle size in the following two ways: (i) it acts as a nucleus of crystallization, and (ii) it condenses or segregates at grain boundaries during the thermal treatments and retains the diffusion necessary for the growth of the crystallites. The compositions containing the larger BaO concentrations ( $\geq 20\text{ mol}\%$ ) probably form thick films of barium oxide-rich material at the grain boundaries which interfere with the crystallization process [10].

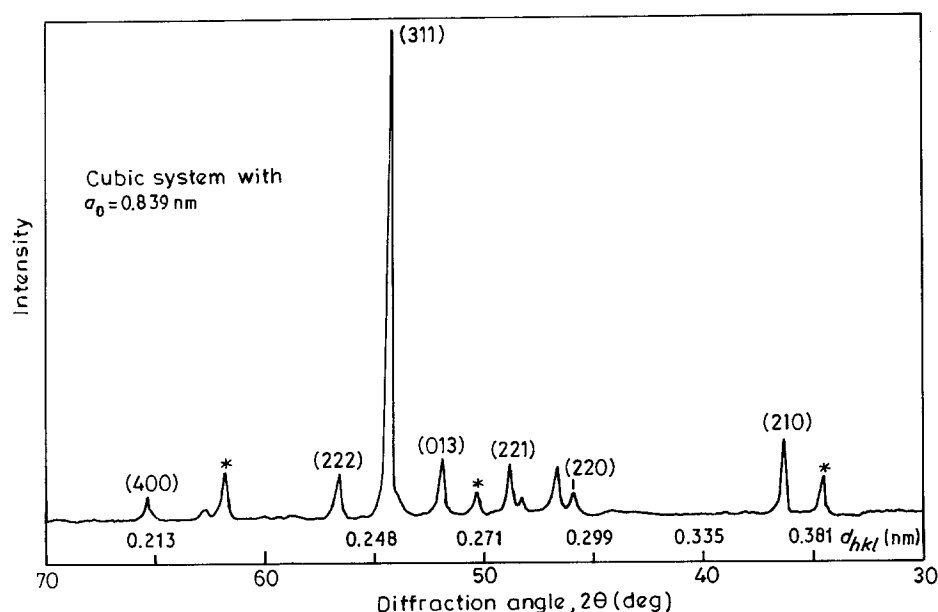


Figure 1 X-ray diffraction patterns for composition series E after the thermal treatment at  $1230^\circ\text{C}/20\text{ h}$ . The lines characteristic of the  $\gamma\text{-Fe}_2\text{O}_3$  crystalline phase are marked by the  $(hkl)$  values. \* These lines are not assigned firmly.

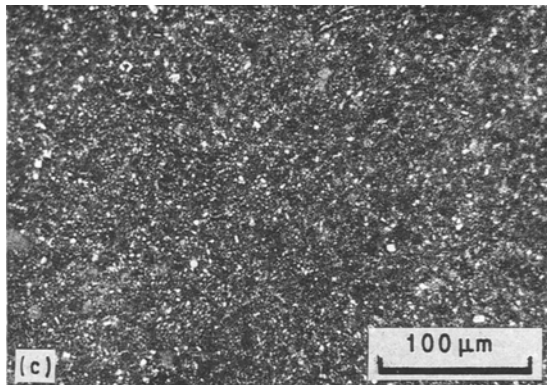
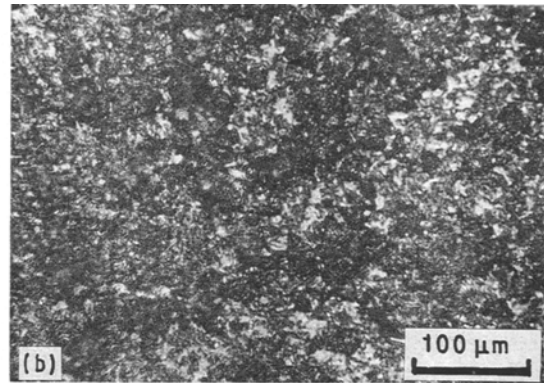
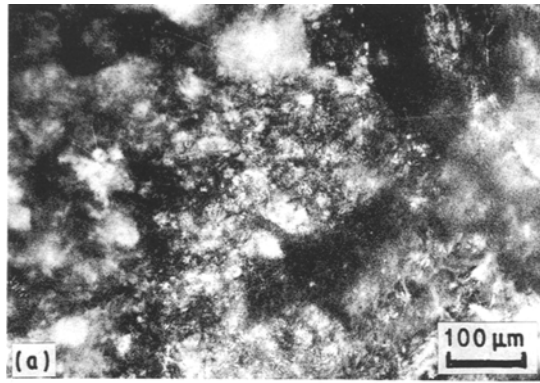


Figure 2 Micrographs showing the effects of BaO addition on the crystalline particle size (white) of  $\gamma\text{-Fe}_2\text{O}_3$  crystallizing in the system subjected to thermal treatment (at  $1230^\circ\text{C}/20\text{h}$ ). The sample contains (a) 5, (b) 8 and (c) 20 mol % BaO.

### 3.2. Magnetic properties

Magnetic moments ( $M_s$ ) of the samples obtained as a function of temperature used for the thermal treatments in the reaction are shown in Fig. 3. The  $M_s$  passes through a maximum value for each of the samples corresponding to a treatment at around  $1230^\circ\text{C}$  for 20 h, ensuring the latter to be the optimum condition for the growth of magnetic particles in the present system. The variation of  $M_s$  (found to be maximum  $\sim 41\text{ e.m.u. g}^{-1}$  for composition series E), however, does not look proportional to the crystallizing mass (see Table II) in the composition series. The crystallites exhibit lower  $M_s$  than that expected for  $\gamma\text{-Fe}_2\text{O}_3$  magnetic particles. This is likely, if BaO participates in the crystallization, leading to a  $\text{Ba}^{2+} \rightleftharpoons \text{Fe}^{3+}$  type substitution reaction in  $\gamma\text{-Fe}_2\text{O}_3$ .

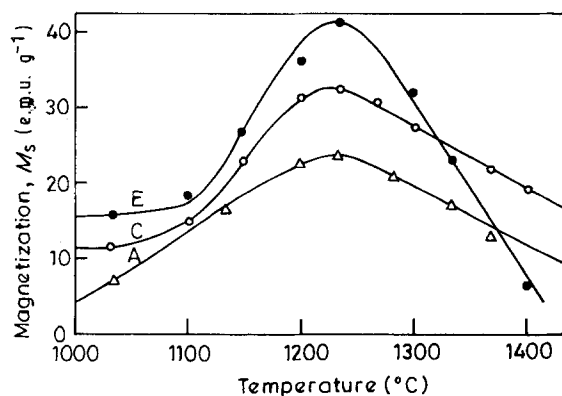


Figure 3 Maximum magnetization ( $M_s$ ) observed as a function of the thermal treatment of samples in the different composition series. All the samples were exposed for 20 h.

The  $\text{Ba}^{2+}$  cations proposed to substitute on the octahedral ( $\text{Fe}^{3+}$ ) sites account for the variation in  $M_s$  compared to  $65\text{ e.m.u. g}^{-1}$  reported for the pure synthesized  $\gamma\text{-Fe}_2\text{O}_3$  [11] observed for these samples. This is consistent with the similar results reported for  $\text{Co}^{2+}$ -substituted  $\gamma\text{-Fe}_2\text{O}_3$  particles [4].

It is interesting that  $H_c$  in these samples (Fig. 4) varies from a few Oersted to  $\sim 3500\text{ Oe}$ , strengthening the wide field of applications of the product. The samples deduced with characteristically large  $H_c$  values ( $\sim 3500\text{ Oe}$ ) appear important for applications as permanent magnets and those with  $H_c \leq 10\text{ Oe}$  for magnetic switching applications [12, 13]. The intermediate  $H_c$  values (i.e. of the order of  $800\text{ Oe}$ ) obtained especially by the thermal treatments at  $\sim 1200^\circ\text{C}/20\text{ h}$  of composition series E, look suitable (except that the particle size of the sample is still larger) for magnetic recording applications. The squareness ratio ( $M_r/M_s$ ) in these samples is found to be  $\sim 0.4$ . More appropriate  $M_r/M_s$  values ( $\geq 0.4$ ) for the high-density recording media [1] are achieved corresponding to thermal treatments given at temperatures much below  $1200^\circ\text{C}$ , but they comprise smaller  $M_s$  values.

The increase in coercivity for barium-modified  $\gamma\text{-Fe}_2\text{O}_3$  particles, compared to that for pure  $\gamma\text{-Fe}_2\text{O}_3$

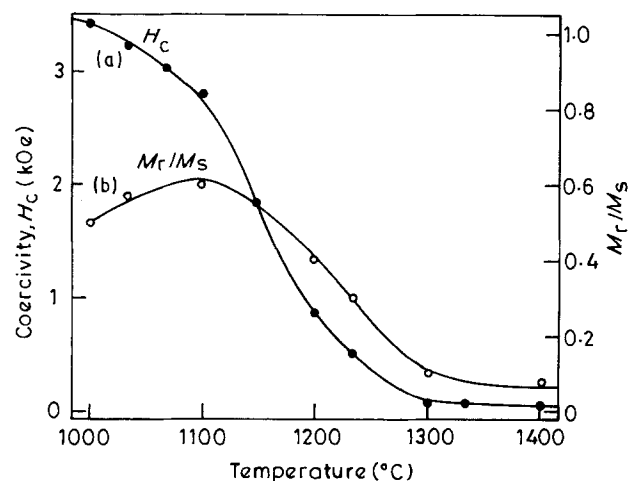


Figure 4 Variation of (a) coercivity and (b) remanent magnetization ( $M_r/M_s$ ) with thermal treatment for the sample series E.

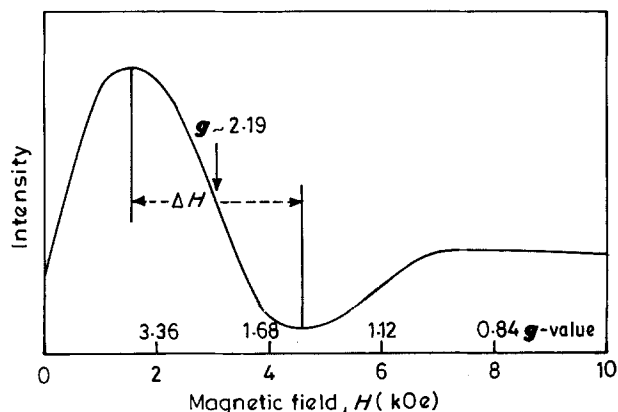


Figure 5 A typical EPR spectrum of composition series E (after treatment at 1230 °C/20 h).

phase ( $H_c \sim 130$  Oe) [11], is believed to arise due to diffusion of  $Ba^{2+}$  cations into the particle core. This is very similar to the results of Takuoka *et al.* [14] for cobalt-adsorbed  $\gamma$ - $Fe_2O_3$  particles by thermal treatment. The data of our X-ray diffraction and magnetization measurements are consistent with the hypothesis that thermal treatment results in (apart from the crystallization of the system) barium-diffusion into the  $\gamma$ - $Fe_2O_3$  particles crystallizing in the system. The latter influences coercivity mainly by modifying the magnetocrystalline anisotropy,  $H_a$  ( $H_a = 2K_1/M_s$ ,  $K_1$  being the uniaxial anisotropy constant) following the coercivity relation [15]

$$H_c = p(H_a - H_b) \quad (1)$$

where  $p$  is a geometrical parameter and  $H_b$  the shape anisotropy factor. This occurs due to the replacement of  $Fe^{2+}$  ions in octahedral sites or occupation of  $Fe^{3+}$  vacancies by  $Ba^{2+}$  ions [12]. A theoretical explanation for this change of  $H_a$  anisotropy could be offered by a "one-ion" model [16] involving spin-orbit coupling of the  $Ba^{2+}$  ions placed in the trigonally symmetric field of the iron oxide. The thermal treatment of the samples at high temperatures ( $\geq 1200$  °C) causes the nucleation centres of  $Ba^{2+}$  to become thermally randomized among different sites, each with different orientation of the trigonal axis, thus decreasing the uniaxial anisotropy and finally  $H_c$ .

### 3.3. Magnetic resonance

Electron paramagnetic resonance spectra of the various samples exhibit a strong resonance at  $g \sim 2.2$

(a typical example is given in Fig. 5), characteristic of the ferrimagnetic resonance of  $Fe^{3+}$  ions [7, 15]. The linewidth ( $\Delta H$ ) varies over the range 3 to 2 kOe, with smaller values noticed for the samples given thermal treatment corresponding to the higher temperatures. Several factors, such as porosity, magnetocrystalline anisotropy ( $H_a$ ), shape anisotropy ( $H_b$ ) and anisotropy due to growth defects, usually contribute to  $\Delta H$  in the polycrystalline ceramic materials. A previous investigation [15] studied the individual effects of these factors in some detail for the crystallization of  $Ca^{2+}$  ferrite as the magnetic particles. The trend observed for  $\Delta H$  in the present investigation thus indicates a lack of porosity anisotropy factors and development of the contribution from the growth defects, mainly due to multidomain nucleation formation [17] in the system for the thermal treatments at high temperatures.

### References

1. S. YOSHII, O. ISHII, S. HATTORI, T. NAKAGAWA and G. J. ISHIDA, *J. Appl. Phys.* **53** (1982) 2556.
2. J. U. LEMKE, *IEEE. Trans. Magn.* **MAG 15** (1979) 1561.
3. A. BEARDSLEY, *ibid.* **MAG 18** (1982) 1191.
4. O. ISHII, F. YOSHIMURA and S. OHARA, *ibid.* **MAG 23** (1987) 1985.
5. B. T. SHIRK and W. R. J. BUESSEM, *Amer. Ceram. Soc.* **53** (1970) 192.
6. O. KUBO, T. IDO and H. YOKOYAMA, *IEEE. Trans. Magn.* **MAG 18** (1982) 1122.
7. S. RAM, D. CHAKRAVORTY and D. BAHADUR, *J. Magn. Mater.* **62** (1986) 221.
8. S. RAM and K. A. NARAYAN, *Ind. Engng Chem. Res.* **26** (1987) 1051.
9. D. E. DAVIES and U. R. EVANS, *J. Chem. Soc.* (also JCPDS file no. 4. 755) (1956) 4373.
10. F. KOOLS, *Adv. Ceram.* **15** (1985) 177.
11. Y. GOTO, *Jpn J. Appl. Phys.* **3** (1964) 742.
12. G. BATE, in "Ferromagnetic Materials", Vol. II, edited by E. P. Wohlfarth (North-Holland, Amsterdam, 1980) pp. 381-507.
13. P. I. SLICK, "Ferromagnetic Materials", Vol. II, edited by E. P. Wohlfarth (North-Holland, Amsterdam, 1980) pp. 189-241.
14. Y. TOKUOKA, H. SUGIHARA, S. OKA and Y. IMAOKA, *J. Chem. Soc. Jpn* **10** (1981) 1564.
15. S. RAM, D. BAHADUR and D. CHAKRAVORTY, *J. Non-Cryst. Solids* **101** (1988) 227.
16. J. C. SLONCZEWSKI, *Phys. Rev.* **110** (1958) 1341.
17. O. KUBO, T. IDO, H. YOKOYAMA and Y. KOIKE, *J. Appl. Phys.* **57** (1985) 4280.

Received 3 August 1989

and accepted 19 February 1990